J. Fluid Mech. (2001), *vol.* 434, *pp.* 181–207. Printed in the United Kingdom

The degeneration of large-scale interfacial gravity waves in lakes

By D. A. HORN, J. IMBERGER AND G. N. IVEY

Centre for Water Research, The University of Western Australia, Nedlands W.A. 6907, Australia

(Received 8 October 1998 and in revised form 12 October 2000)

Mechanisms for the degeneration of large-scale interfacial gravity waves are identified for lakes in which the effects of the Earth's rotation can be neglected. By assuming a simple two-layer model and comparing the timescales over which each of these degeneration mechanisms act, regimes are defined in which particular processes are expected to dominate. The boundaries of these regimes are expressed in terms of two lengthscale ratios: the ratio of the amplitude of the initial wave to the depth of the thermocline, and the ratio of the depth of the thermocline to the overall depth of the lake. Comparison of the predictions of this timescale analysis with the results from both laboratory experiments and field observations confirms its applicability. The results suggest that, for small to medium sized lakes subject to a relatively uniform windstress, an important mechanism for the degeneration of large-scale internal waves is the generation of solitons by nonlinear steepening. Since solitons are likely to break at the sloping boundaries, leading to localized turbulent mixing and enhanced dissipation, the transfer of energy from an initial basin-scale seiche to shorter solitons has important implications for the lake ecology.

1. Introduction

Since internal waves play an important role in driving mixing in stratified lakes and reservoirs, our efforts to predict water quality require an understanding of the dynamics of the internal wavefield (Mortimer & Horn 1982; Imberger 1994). Considerable progress has been made on quantifying the sources and sinks of energy, but surprisingly little work has been undertaken on the way in which energy is transferred within the internal wavefield.

In lakes the major source of energy for the internal wavefield is the action of the wind over the surface of the lake, generating large-scale internal gravity waves with relatively low frequency. In small to medium sized lakes, in which the effects of the Earth's rotation can be neglected, the dominant response is a basin-scale standing wave known as an internal seiche (Mortimer 1974). Even when the wind does not blow for sufficient duration to generate a true standing wave (Spigel & Imberger 1980), the horizontal extent of the thermocline displacement is of the same order as the basin length and we will refer to these waves as basin-scale internal waves. For internal gravity waves, the Earth's rotation can be neglected in lakes with widths less than the Rossby radius of deformation which for mid-latitude lakes equates to widths of less than approximately 4–5 km (Hutter 1991). In lakes in which the Earth's rotation is important, the response to an applied wind stress is the generation of Kelvin and Poincaré waves (Mortimer 1974; Saggio & Imberger 1998). In most lakes the wind can also generate topographic waves (very low-frequency rotational waves).

Perhaps surprisingly, these rotational waves can exist in lakes in which the Earth's rotation can be neglected for internal gravity waves and, in some lakes, may play an important role in the dynamics (Stocker & Hutter 1987). However, topographic waves in lakes are still poorly understood and their identification from field data is difficult. In this paper we neglect topographical waves, considering only internal gravity waves, and we neglect the Earth's rotation so the analysis applies only to small to medium sized, or long narrow lakes. In particular, we consider the situation where the wind stress is relatively uniform and the surrounding orography is simple.

Although the wind energizes the low-frequency basin-scale internal waves, field experiments indicate that the internal wavefield has a continuous spectrum ranging from these low-frequency standing waves through to waves with frequencies approaching the buoyancy frequency (e.g. Thorpe 1977; Thorpe *et al.* 1996; Saggio & Imberger 1998). Furthermore, field observations show that the wind-forced basin-scale waves decay at a rate far greater than can be accounted for simply by internal dissipation (Imberger 1994; Stevens *et al.* 1996). The observed decay times require that other mechanisms must act to transfer energy from these basin-scale waves to either smaller-scale waves or to turbulent scales. Possible mechanisms that are likely to result in such energy transfers include: (i) nonlinear steepening, (ii) shear instabilities, (iii) shoaling and reflection at sloping boundaries, and (iv) interaction with topography.

Field studies have found that large-scale internal waves often take the form of an internal surge or a packet of internal solitons, generated by the nonlinear steepening of an initial finite-amplitude wave (e.g. Hunkins & Fliegel 1973; Thorpe 1977; Farmer 1978; Wiegand & Carmack 1986). Since these solitons are of much shorter length than the wind-induced initial large-scale thermocline displacement, their generation results in a transfer of energy within the internal wavefield from large to smaller scales. Numerical modelling has also demonstrated the importance of nonlinear steepening of initial basin-scale waves and the generation of small-scale nonlinear waves by wind (Hutter *et al.* 1998).

Field observations also suggest that the shoaling and reflection of large-scale internal waves at lake boundaries plays a major role in the generation of smaller-scale internal waves. Large internal waves can interact with local topography such as sills and headlands, radiating high-frequency waves (Thorpe 1998; Thorpe *et al.* 1996). Imberger (1994) postulated that the waves identified by the high-frequency peaks in the Lake Biwa isotherm displacement spectra were generated by the interaction of the basin-scale waves with the lake boundaries. The shoaling and reflection of internal waves is also thought to play a major role in driving the turbulence in the benthic boundary layer (Ivey & Nokes 1989; Imberger 1994). Whether by the generation of smaller-scale internal waves or by driving turbulence in the benthic boundary layer, interaction with the boundaries contributes to the decay of large internal waves.

Observations in the ocean (Woods 1968) and in lakes (Thorpe *et al.* 1977) have confirmed that propagating internal waves can induce sufficient shear to cause Kelvin–Helmholtz instabilities. The turbulent collapse of Kelvin–Helmholtz billows leads in turn to patches of high dissipation and mixing, the whole chain of events thus providing a mechanism for the transfer of energy from the large-scale waves to mixing at smaller scales. Whereas the maximum shear for propagating internal waves is at the crests and troughs, the maximum shear for standing waves is at the node points. Although laboratory studies have confirmed that standing waves may generate shear instabilities (Thope 1968), no field observations have been reported of Kelvin–Helmholtz billows at the node of a basin-scale seiche.

The relative importance of each of these mechanisms and the energy transfers

associated with them in lakes are yet to be quantified. Since in lakes exposed to a uniform wind stress most energy enters the internal wavefield at the large scale (Mortimer 1974), we examine here the degeneration of the large-scale waves and the resulting transfer of energy from these waves to smaller scales. In particular, we examine the degeneration of an initial basin-scale internal standing wave that is generated by the relaxation of an initially tilted density interface. In § 2 we use a simple two-layer rectangular model to derive the timescales over which these degeneration processes operate. The relative ordering of these timescales is then used to identify regimes in which particular mechanisms would be expected to dominate the degeneration of basin-scale internal waves. In §§ 3 and 4 we compare our model predictions with the results of laboratory experiments and field observations to demonstrate the applicability of the regimes. We then briefly discuss the consequences of these processes for the energy cascade and for water quality in lakes.

2. Derivation of timescales and regimes

2.1. *Initial conditions: the set-up of the interface*

Field observations (e.g. Mortimer 1952; Imberger 1985) and laboratory experiments (e.g. Wu 1977; Monismith 1986; Stevens & Imberger 1996) have confirmed that wind blowing over the surface of a lake transports the less-dense surface water towards the leeward end, tilting the free surface up and the thermocline down. The response is complicated by such factors as the unsteady nature of the wind, deepening of the surface layer and by any pre-existing background circulation and internal wavefield.

A key parameter determining the response of a lake to a wind event is the Wedderburn number, W (Thompson & Imberger 1980), defined as the ratio of the surface layer Richardson number to the aspect ratio

$$W = \frac{Ri}{L/h_1} = \frac{g'h_1^2}{u_*^2 L} \tag{2.1}$$

where u_* is related to the applied wind stress by $\tau = \rho u_*^2$, h_1 is the depth of the surface layer, $g' = (\Delta\rho/\rho_0)g$, $\Delta\rho$ is the density difference between the epilimnion and the hypolimnion, ρ_0 is some reference density and L the length of the lake. Spigel & Imberger (1980) classified the response of a lake to a given wind event into four regimes. Of particular importance is the regime boundary at $W \approx 1$. For $W \leqslant 1$ (Spigel & Imberger's regimes 1 and 2) the steady state does not generally result in a tilted thermocline but in substantial or complete mixing of the lake. However, for $W > 1$ (Spigel & Imberger's regimes 3 and 4) the interface oscillates about an equilibrium tilt of $\theta \approx u_*^2/g'h_1$. If the wind continues to blow, the seiching is eventually damped and a steady-state tilt results.

When the wind stress is removed the lake adjusts to return to its original state with the thermocline horizontal. The amplitude of the resulting seiche will depend on the strength and duration of the wind event but is limited by the maximum interface displacement (Monismith 1987)

$$\zeta_{\max} = \frac{Lu_*^2}{g'h_1}. \tag{2.2}$$

From (2.1) we have $\zeta_{\max}/h_1 = W^{-1}$.

The analysis and laboratory experiments described below assume an initial condition consisting of a tilted density interface and apply equally to basin-scale internal

waves generated during the set-up of the thermocline and to those generated by the subsequent relaxation of the thermocline after the removal of the applied wind stress.

2.2. *Two-layer model*

Before proceeding to investigate the mechanisms that contribute to the degeneration of the internal seiche it is useful to introduce a simple model from which the major features of the flow can later be extracted. We initially consider a two-layer rectangular basin in which the subscripts $i = 1$ and 2 are used to denote the upper and lower fluids respectively, so that the fluid in each layer has a constant density ρ_i and an equilibrium depth h_i. We shall use the spatial coordinates x and z with z being directed vertically upward. The deflection of the free surface is given by $\zeta_1(x,t)$ and that of the internal interface by $\zeta_{12}(x,t)$.

In a two-dimensional non-rotating system, ignoring viscous effects, we consider small-amplitude motions and make the hydrostatic approximation. It is useful to introduce the layer average velocities U_i where

$$U_i = \frac{1}{h_i}\int_{\text{layer}} u_i \,\mathrm{d}z.$$

The horizontal momentum equations for each layer can now be written (e.g. Spigel 1978) as

$$\frac{\partial U_1}{\partial t} = g\frac{\partial \zeta_1}{\partial x}, \tag{2.3}$$

$$\frac{\partial U_2}{\partial t} = g\frac{\partial \zeta_1}{\partial x} + g'\frac{\partial \zeta_{12}}{\partial x}. \tag{2.4}$$

Since the deflection of the free surface is small compared with the deflection of the internal interface, conservation of volume can be approximated as $h_1 U_1 = -h_2 U_2$. Making use of conservation of volume to eliminate U_1, (2.3) and (2.4) can be combined to give

$$\frac{\partial U_2}{\partial t} + \frac{g' h_1}{H}\frac{\partial \zeta_{12}}{\partial x} = 0. \tag{2.5}$$

Applying conservation of volume to the lower layer we also have

$$\frac{\partial U_2}{\partial x} + \frac{1}{h_2}\frac{\partial \zeta_{12}}{\partial t} = 0. \tag{2.6}$$

We can combine (2.5) and (2.6) in the form

$$\left(\frac{\partial U_2}{\partial t} + c_o\frac{\partial U_2}{\partial x}\right) + \frac{c_o}{h_2}\left(\frac{\partial \zeta_{12}}{\partial t} + c_o\frac{\partial \zeta_{12}}{\partial x}\right) = 0 \tag{2.7}$$

where c_o is the linear long-wave speed

$$c_o = \pm\left(g'\frac{h_1 h_2}{H}\right)^{1/2}. \tag{2.8}$$

We recognize $\mathrm{D}/\mathrm{D}t = \partial/\partial t \pm c_o \partial/\partial x$ as the directional derivative along the characteristic curves $\mathrm{d}x/\mathrm{d}t = \pm c_o$, so we can rewrite equation (2.7) as

$$\frac{\mathrm{D}}{\mathrm{D}t}\left(U_2 \pm \frac{c_o}{h_2}\zeta_{12}\right) = 0 \quad \text{along} \quad \frac{\mathrm{d}x}{\mathrm{d}t} = \pm c_o. \tag{2.9}$$

We can now determine the values of U_2 and ζ_{12} at some point (x,t) by integrating

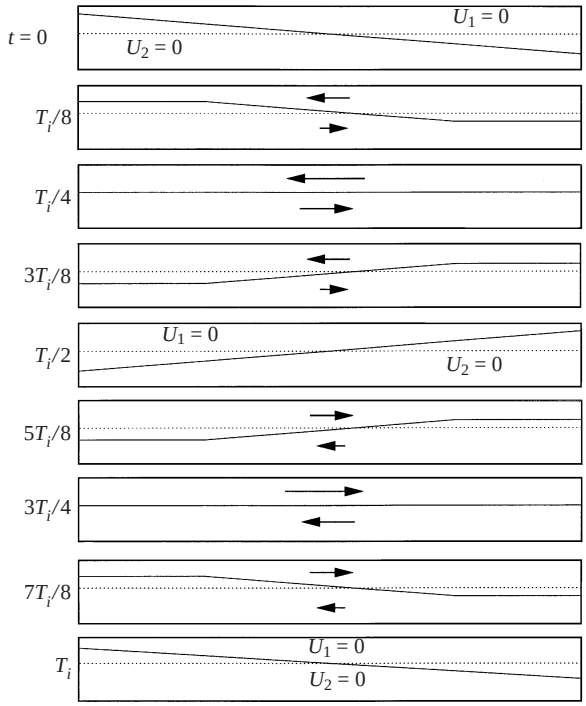

FIGURE 1. Schematic illustration of the basin-scale wave resulting from a tilted interface. The interface position and layer velocities are shown at intervals over one internal wave period T_i. The maximum layer velocities occur at $t = T_i/4$ and $t = 3T_i/4$. Note the asymmetry in the layer velocities since $h_1U_1 = h_2U_2$ and $h_1 < h_2$.

equation (2.9) along the characteristic curves that pass through the point (x, t) and by using the initial conditions. Conservation of volume then yields U_1.

The initial conditions used in our experimental study, described in § 3, consist of a tilted interface, where the maximum displacement of the interface is denoted by η_o, and with no motion so that $U_1 = U_2 = 0$. While these conditions exactly match the tilting tube experiments, they also approximate the theoretical linear steady-state response of a reservoir to an applied uniform wind stress in the absence of entrainment (Spigel & Imberger 1980). The main features of the flow resulting from these initial conditions are summarized in figure 1. The flow is periodic with a period $T_i = 2L/c_o$ with the maximum velocities occurring when the interface is horizontal at $t = T_i/4, 3T_i/4, 5T_i/4 \ldots$. For initial conditions consisting of a tilted interface, the layer velocities increase linearly from zero at the ends of the basin to a maximum at the centre of the tank, so that

$$U_i = \hat{U}_i \frac{2x}{L} \quad \text{for} \quad x \leqslant \frac{L}{2} \tag{2.10}$$

where $\hat{U}_i$ is the layer velocity at the centre of the basin. Before the flow reverses at $t = T_i/4$, the layer velocities at the centre of the tank are given by

$$\hat{U}_1 = g' \frac{h_2}{H} \frac{2\eta_o}{L} t, \tag{2.11}$$

$$\hat{U}_2 = -g' \frac{h_1}{H} \frac{2\eta_o}{L} t. \tag{2.12}$$

2.3. *Shear instabilities*

The internal standing wave shown in figure 1 results in substantial interfacial shear that is periodic and has a maximum value at the node when the interface is horizontal. From (2.11) and (2.12), for $t \leqslant T_i/4$ the shear at the node is given by

$$\Delta\hat{U} = \hat{U}_1 - \hat{U}_2 = g' \frac{2\eta_o}{L} t. \tag{2.13}$$

The lengthscale over which the velocity shear occurs is imposed by the finite thickness of the density interface, δ_ρ, so we can define a local Richardson number

$$Ri = \frac{g'\delta_\rho}{(\Delta\hat{U})^2}. \tag{2.14}$$

Based on a stability criterion of $Ri > 0.25$ and the assumption that the shear is steady, the minimum shear necessary for Kelvin–Helmholtz billows is thus $\Delta\hat{U} = 2(g'\delta_\rho)^{1/2}$. Since the wave-induced shear initially increases with time, the flow is always stable before the time

$$T_{KH} = \frac{L}{\eta_o}\left(\frac{\delta_\rho}{g'}\right)^{1/2}. \tag{2.15}$$

If $T_{KH} > T_i/4$ the flow will remain stable since the shear first reaches its maximum value at $T_i/4$, although we note (2.15) takes no account of the finite time required for the growth of the unstable waves that eventually form the billows. In a series of laboratory experiments using a tilting tube (Thorpe 1971) found that for accelerating flows the Richardson number at which billows appeared was well below the critical value of 0.25, suggesting that (2.15) will underestimate the time at which shear instabilities would be observed.

The quasi-steady approximation is good only if the timescale for the growth of billows is much shorter than $T_i/4$. Corcos & Sherman (1976) estimated that the time for billows to grow to maximum amplitude was $5\Delta U/g'$, which for the basin-scale wave is given by $(2.5\eta_o/L)T_i$. Thus, for the steady flow assumption to be valid we require $\eta_o/L \ll 0.1$, which will be true for most lakes and for our laboratory experiments.

Equation (2.15) also ignores viscous effects which act to stabilize the flow. Viscosity reduces the actual velocities below those predicted by the inviscid model on which the analysis is based and reduces the velocity gradients across the interface, increasing Ri (Thorpe 1971). Using the relation given in the appendix of Thorpe (1971), the time at which the billows are expected will increase by the factor given by

$$Q = \frac{1}{2}\left\{1 + \left(1 + 4\left(\frac{\nu t}{\delta_\rho^2}\right)\right)^{1/2}\right\}. \tag{2.16}$$

The shear instability timescale T_{KH} applies to basin-scale standing internal waves where the maximum shear is located at the node. Kelvin–Helmholtz instabilities can still be generated by the shear induced by smaller-scale propagating internal waves. Large solitary waves and surges, for example, are able to generate considerable interfacial shear, especially if superimposed on the background shear of a basin-scale seiche.

2.4. *Nonlinear steepening*

Most previous analytical studies of basin-scale internal waves in lakes have been based on linear theory. However, field observations have shown that the amplitude of

the internal seiche is generally large enough that nonlinear effects become significant (e.g. Hunkins & Fliegel 1973; Thorpe 1977; Farmer 1978; Mortimer & Horn 1982; Wiegand & Carmack 1986). Furthermore, numerical studies have confirmed the importance of nonlinear effects in generating the small-scale features that are typically observed in field data (Hutter *et al.* 1998). Hammack & Segur (1978) present modelling criteria for long surface water waves, the results of which are useful when considering the importance of nonlinear and dispersive effects for long internal gravity waves.

The initial steepening of a finite-amplitude long wave due to nonlinear effects can be described by the nonlinear non-dispersive wave equation (e.g. Hammack & Segur 1978; Long 1972)

$$\frac{\partial \eta}{\partial t} + c_o \frac{\partial \eta}{\partial x} + \alpha \eta \frac{\partial \eta}{\partial x} = 0 \tag{2.17}$$

where $\alpha = \frac{3}{2} c_o (h_1 - h_2)/h_1 h_2$. Here η is defined as positive upwards, so for the case of a thin upper layer ($h_1 < h_2$), only an initial wave of depression ($\eta < 1$) will steepen. Balancing the unsteady and nonlinear terms leads to a steepening timescale T_s for a basin-scale wave of length L and amplitude η_o

$$T_s \sim \frac{L}{\alpha \eta_o}. \tag{2.18}$$

This is the classical result (Lighthill 1978, e.g. see equation 188) and is similar to the sorting time demonstrated by Hammack & Segur (1974) and the breaking timescale derived by Farmer (1978). We will initially take the constant of proportionality to be 1 and will verify this value using the experimental data presented in § 3.2. The rate of nonlinear steepening depends on $|\eta_o/h_1|$, increasing as the surface layer becomes thin or as the amplitude of the initial basin-scale wave increases. Note that when the interface is at mid-depth the nonlinear coefficient vanishes ($\alpha = 0$).

As the wave steepens its horizontal lengthscale decreases until the dispersive terms can no longer be neglected (see Hammack & Segur 1978). Eventually, a balance between nonlinear steepening and dispersion leads to the evolution of solitary waves, a process described by the Korteweg–de Vries (KdV) equation

$$\frac{\partial \eta}{\partial t} + c_o \frac{\partial \eta}{\partial x} + \alpha \eta \frac{\partial \eta}{\partial x} + \beta \frac{\partial^3 \eta}{\partial x^3} = 0 \tag{2.19}$$

where $\beta = \frac{1}{6} c_o h_1 h_2$. In this way, large-scale waves can degenerate on the steepening timescale T_s into solitary waves, transferring energy within the internal wavefield from the basin scale to shorter waves.

2.5. *Internal bores*

Field studies have sometimes described the passage of propagating internal hydraulic jumps or bores, so we consider whether these features could be associated with the degeneration of an initial seiche. In this paper we use the terms *internal hydraulic jump* and *internal bore* to describe the nonlinear front generated by supercritical conditions. These are not to be confused with the term *internal surge* which we use to describe a steep fronted nonlinear wave that is not necessarily the result of supercritical conditions but is usually due to the nonlinear steepening of a finite-amplitude wave.

In a two-layer model, when the initially inclined interface relaxes, the velocities in each layer are in opposite directions and the velocity is greatest in the thinner layer. We can define upper and lower layer Froude numbers as $F_1^2 = U_1^2/g'h_1$ and $F_2^2 = U_2^2/g'h_2$, in which case the critical condition is determined by $F_1^2 + F_2^2 = 1$ (Wood

& Simpson 1984). Since the layer velocities have a maximum value in the centre of the basin and are zero at the ends, if the amplitude of the motion is sufficiently great, the flow may be supercritical ($F_1^2 + F_2^2 > 1$) over some region in the middle of the basin but must be subcritical at each of the ends. An internal hydraulic jump, or bore, links the supercritical region with the downstream (relative to the fast flowing thin layer) subcritical region; no jump is required to link the upstream (relative to the thin layer) subcritical region with the supercritical region. The time at which the flow first becomes supercritical can be calculated by setting $\hat{U}_1^2/g'h_1 + \hat{U}_2^2/g'h_2 = 1$, where $\hat{U}_1$ and $\hat{U}_2$ are given by (2.11) and (2.12). After some manipulation, it can be shown that the time at which the flow becomes supercritical is

$$T_b = \frac{T_i}{4}\frac{h_1}{\eta_o}\left(\frac{Hh_2^2}{h_1^3 + h_2^3}\right)^{1/2}. \tag{2.20}$$

Since the flow is periodic, the layer velocities initially increase until a time $t = T_i/4$ and then decrease until they reverse direction at $t = T_i/2$; if $T_b > T_i/4$ the flow never becomes supercritical and a bore of this type will not form.

An important property of hydraulic jumps and bores is that they are associated with an energy loss across the jump. This energy can be lost to dissipation and mixing in the case of a turbulent bore, to waves in the case of an undular bore, or to a combination of these. As energy is lost the bore evolves into a train of solitons, transferring energy from the basin-scale wave to waves of much shorter wavelength. Although the solitons that evolve from the supercritical condition are very similar to the waves generated by the nonlinear steepening of the initial basin-scale wave, the generation mechanisms are quite different in the two cases.

2.6. *Viscous damping*

The analysis so far has ignored viscous damping. A useful dissipative timescale is the e-folding timescale for the amplitude decay of an initial internal standing wave:

$$T_d = \frac{T_i}{\gamma_d} \tag{2.21}$$

where γ_d is the decay modulus and is a measure of the energy lost during one internal wave period, such that $2\gamma_d = dE/E$ (Keulegan 1959). Spigel & Imberger (1980) estimated γ_d for lakes by balancing the energy dissipated in the turbulent boundary layer with the energy of the internal seiche. They demonstrated that the decay could be described well by the simple estimate of γ_d given by

$$\gamma_d = \frac{\delta_b A_b}{V} \tag{2.22}$$

where the thickness of the turbulent boundary layer is estimated using $\delta_b = U_{\max} T_i^{1/2} e/(471\nu^{1/2})$ and e is the sand grain roughness, A_b is the area of the solid boundary and V the volume of the lake.

For the laboratory experiments described in § 3 we must also consider the losses at the rigid lid and in the interfacial shear layer (since the interface thickness is of the same order as the boundary layers). We therefore derive a separate expression for the decay modulus for the laboratory experiments based on the two-layer model described in § 2.2.

The average dissipation of energy E per unit area in an oscillatory boundary layer

over one period is given by (Batchelor 1967)

$$\frac{\mathrm{d}E}{\mathrm{d}t} = -\frac{\mu U^2}{2\delta_\rho} \tag{2.23}$$

where μ is the viscosity, and U is the maximum velocity outside the boundary layer. In the laboratory the thickness of the laminar boundary layer is given by $\delta_b = (\nu T_i/\pi)^{1/2}$ Batchelor 1967. For the internal shear layer the velocity scale is ΔU, and the lengthscale can be approximated by the interface thickness, δ_ρ.

For the linear two-layer model described in § 2.2, (2.23) can be integrated over the area of the solid boundaries for each layer (neglecting the endwalls), A_{b_i}, and over the area of the interface, A_ρ. Since, for the linear standing wave generated by a tilted interface, $U_i = \hat{U}_i 2x/L$ ($x \leqslant L/2$) and $U_1 h_1 = -U_2 h_2$ it can be shown that

$$\begin{aligned}\frac{\mathrm{d}E}{\mathrm{d}t} &= -\int_{A_{b_1}} \frac{\mu U_1^2}{2\delta_b}\mathrm{d}A - \int_{A_{b_2}} \frac{\mu U_2^2}{2\delta_b}\mathrm{d}A - \int_{A_\rho} \frac{\mu \Delta U^2}{2\delta_\rho}\mathrm{d}A \\ &= -\frac{\mu L}{6\delta_b}(\hat{U}_1^2(2h_1 + B) + \hat{U}_2^2(2h_2 + B)) - \frac{\mu L}{6\delta_\rho}(\Delta\hat{U}^2)B \\ &= -\frac{\mu L \hat{U}_2^2}{6\delta_b}\left(\left(\frac{h_2}{h_1}\right)^2 (2h_1 + B) + (2h_2 + B)\right) - \frac{\mu L \Delta\hat{U}^2}{6\delta_\rho}B \end{aligned} \tag{2.24}$$

where $A_{b_i} = L(2h_i + B)$, $A_\rho = LB$ and L and B are the length and width of the fluid. The first term on the right-hand side of (2.24) is the loss at the solid boundaries and the second term is the loss in the interfacial shear layer.

The total energy of the standing internal wave is given by

$$E = \frac{\rho_o BL}{6}\left(\hat{U}_1^2 h_1 + \hat{U}_2^2 h_2\right) = \frac{\rho_o BL}{6}\frac{h_2}{h_1}\hat{U}_2^2. \tag{2.25}$$

Following Spigel (1980), we can use (2.24) and (2.25) to estimate the fraction of wave energy dissipated each wave period. After some manipulation and recalling that $\delta_b = (\nu T_i/\pi)^{1/2}$ it can be shown that

$$\frac{\mathrm{d}E}{E} = \frac{\pi\delta_b A_b}{V} + \frac{\nu H T_i}{\delta_\rho h_1 h_2} = 2\gamma_d \tag{2.26}$$

where A_b is the total area of the solid boundaries and V is the total volume. For determining the damping timescale we use (2.26) for the laboratory experiments and (2.22) when considering field data.

2.7. *Regimes*

Depending on the relative ordering of the degeneration timescales described above, a number of regimes can be defined in which a particular mechanism is expected to dominate. In a continuously accelerating flow the fastest timescales would be those associated with supercritical flow (T_b) when h_1/H is less than about 0.25 and shear instabilities (T_{KH}) for h_1/H is greater than about 0.25 (the transition also depends on the interface thickness). However, in the case where the flow is generated by a basin-scale standing wave, the periodic nature of the flow limits the magnitude of the layer velocities. This restricts the regimes in which bores or billows will be found to those in which $T_{KH} < T_i/4$ or $T_b < T_i/4$ whereas nonlinear steepening and viscous damping can operate continuously over multiple wave periods.

By equating timescales, the regime boundaries can be calculated in terms of the

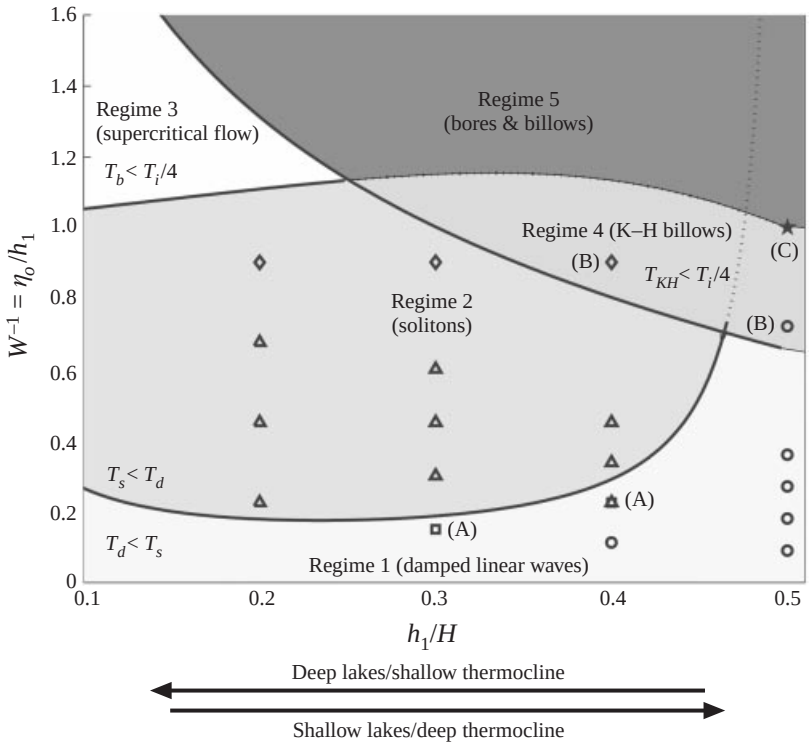

FIGURE 2. The regime boundaries for the laboratory experiments, plotted in terms of the amplitude ratio of the initial basin-scale wave η_o/h_1 and the depth ratio h_1/H. A typical interface thickness $\delta_\rho \approx 1$ cm was used to determine the timescales T_{KH} and T_d. The laboratory observations described in §3.2 are also plotted (⋆, K-H billows and bore; ◇, broken undular bore; △, solitons; □, steepening; ○, damped linear waves).

amplitude of the initial basin-scale seiche η_o and the depth of the interface h_1. Since the magnitude of the coefficient of the nonlinear term in (2.17) depends on the ratios η_o/h_1 and h_1/H, we choose these as axes for the regime diagram in figure 2. The damping timescale T_d and the shear instability timescale T_{KH} both depend on other characteristics of the lake and stratification (in particular on L, g' and δ_ρ), so the regime boundaries need to be calculated individually for each lake. As an example, figure 2 has been calculated for the laboratory experiments. In §4 we present regime diagrams calculated for several lakes.

We now define five regimes in each of which different mechanisms are expected to dominate.

2.7.1. *Regime 1 (damped basin-scale wave): $T_d < T_s$*

When the amplitude of the initial basin-scale wave is too small to generate shear instabilities ($T_{KH} > T_i/4$) or supercritical conditions ($T_b > T_i/4$), the degeneration of the initial wave is determined by the competition between viscous damping and nonlinear steepening. If the timescale for damping is shorter than the timescale for nonlinear steepening, the amplitude of the initial internal seiche will be damped before it can steepen and evolve into solitons. The basin-scale wave retains many of the characteristics of the theoretical linear wave and linear analysis captures the dynamics of the resulting mean flow. The largest-amplitude seiche that will be damped

before it evolves into solitons is determined by setting $T_d = T_s$ using (2.21) and (2.18):

$$W^{-1} = \frac{\eta_o}{h_1} = \frac{\gamma_d}{3}\left(\frac{h_2}{h_2 - h_1}\right) \tag{2.27}$$

where γ_d is defined by (2.26) in our laboratory experiments and by (2.22) in lakes. We note that γ_d is a function of the T_i, and therefore of the length of the lake and the strength of the stratification (and of δ_ρ in the laboratory experiments). Figure 2 shows that the response is expected to be linear only for very small amplitudes, or when the interface is near the mid-depth. In this regime the energy is dissipated directly from the basin-scale wave without cascading through smaller wavelengths.

2.7.2. *Regime 2 (solitons): $T_s < T_d$*

In this regime the amplitude of the initial basin-scale wave is still too small to generate shear instabilities ($T_{KH} > T_i/4$) or supercritical conditions ($T_b > T_i/4$), but the initial basin-scale wave will steepen more quickly than it is damped and will evolve into a train of solitons. The smallest-amplitude seiche that will evolve into solitons is given by (2.27). Figure 2 shows that Regime 2 covers most of the parameter space for our laboratory experiments, so that nonlinear steepening is expected to be an important mechanism for the degeneration of the initial standing waves.

It can be shown that for many natural lakes the boundary between Regimes 1 and 2 occurs between $W = 5$ and $W = 10$. The importance of nonlinearity in these systems raises questions about the initial set-up of the thermocline, the accepted theory of which is based on assumptions of linearity. This matter will be discussed in more detail in § 5.

In this regime energy is transferred within the internal wavefield from the low-frequency basin-scale seiche to much shorter waves with higher frequencies.

2.7.3. *Regime 3 (supercritical flow): $T_b < T_i/4$, $T_s > T_i/4$*

This defines the regime in which the flow becomes supercritical before the initial wave can degenerate by any other mechanism and a bore forms. This process is usually accompanied by significant dissipation and mixing due to localized shear-induced turbulence associated with the bore. Setting T_b to its maximum value of $T_i/4$ yields the amplitude η_o of the smallest seiche that might degenerate into an internal surge or bore:

$$W^{-1} = \frac{\eta_o}{h_1} = \left(\frac{h_2^2 H}{h_1^3 + h_2^3}\right)^{1/2}. \tag{2.28}$$

We add the condition that $T_{KH} > T_i/4$ to exclude conditions in which both billows and bores might exist together (Regime 5).

For $h_1 \ll H$, 2.28 can be simplified to $W^{-1} \approx 1$, under which conditions the thermocline reaches the surface. Upwelling leads to the development of a highly nonlinear density front causing mixing and deepening of the surface layer (Monismith 1986), all of which conspire to disrupt wave motion.

2.7.4. *Regime 4 (Kelvin–Helmholtz billows): $T_{KH} < T_i/4$, $T_b > T_i/4$*

In this regime, if $T_{KH} < T_i/4$ the wave-induced shear across the thermocline causes the local Richardson number to fall below 0.25 and Kelvin–Helmholtz billows form at the node. By setting $T_{KH} = T_i/4$ in (2.15) the minimum-amplitude seiche that will

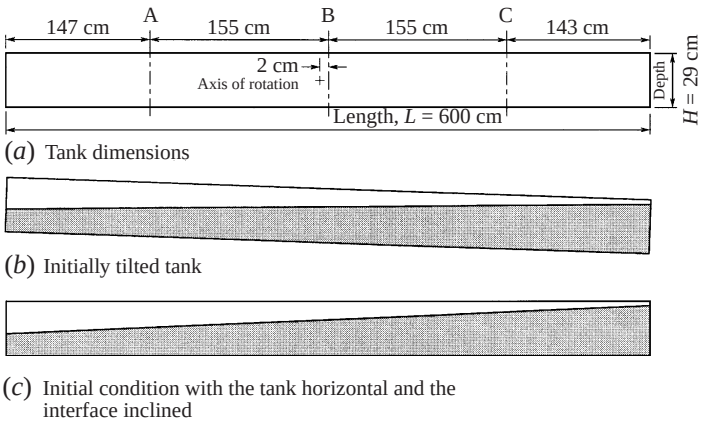

FIGURE 3. Schematic diagram of the experimental set-up. The ultrasonic wavegauges were located at the positions marked A, B and C. (b, c) The tank and the density structure immediately before and after an experiment commences.

generate billows is given by

$$W^{-1} = \frac{\eta_o}{h_1} = \frac{2}{Q}\left(\frac{\delta_\rho h_2}{H h_1}\right)^{1/2} \tag{2.29}$$

where Q, from (2.16), has been added to take account of viscosity. We add the condition that $T_b > T_i/4$ to exclude conditions in which both billows and bores might exist together (Regime 5).

The stability of the interface to Kelvin–Helmholtz billowing is determined by the depth and thickness of the interface. For a given interface thickness, the minimum-amplitude seiche that will cause billowing decreases as the depth of the surface layer increases. Shear instabilities generated by a basin-scale standing wave can only be expected for large-amplitude waves when the Wedderburn number is greater than about 1, although slightly smaller angles of tilt may generate sufficient shear when the interface is near mid-depth. When shear instabilities do occur, the turbulent collapse of the billows leads to a transfer of energy from the initial wave directly to turbulent scales and to an increase in the background potential energy of the stratification.

2.7.5. *Regime 5 (bores and billows): $T_{KH} < T_i/4$, $T_b < T_i/4$*

For large initial interface tilts (small Wedderburn numbers) it is possible that the layer velocities can be supercritical and the shear sufficient to generate billows. In these cases both mechanisms happen relatively quickly (faster than $T_i/4$). Whereas the supercritical bores appear and propagate from the ends of the basin, any billowing will first occur at the central node of the basin-scale wave. Regime 5 describes conditions under which both these mechanisms can occur simultaneously. It is restricted to conditions that might result from very strong winds causing upwelling of the thermocline.

3. Laboratory experiments

3.1. *Experimental set-up*

The laboratory experiments were carried out in a fully enclosed clear acrylic tank 600 cm long, 29 cm deep and 30 cm wide. The tank could rotate about a horizontal

axis approximately through its centre so that the interface could be initially tilted. A schematic diagram of the tank is shown in figure 3.

To establish the stratification the tank was tilted through its maximum angle (approximately 23°) and partly filled with the volume of fresh water necessary for the upper layer. Salt water at the correct density was then allowed to slowly flow into the bottom of the tilted tank, underneath the previous lighter layer. For flow visualization the interface or one of the layers was dyed. When the tank was completely filled it was slowly rotated to a horizontal position and the density profile measured by vertically traversing a conductivity sensor and thermistor through the tank. The slow rotation of the tank to a horizontal position stretched the isopycnal surfaces, reducing the interface thickness and increasing the density gradient within the interface. Using this method, initial interface thicknesses of less than 1 cm were consistently achieved. The tank was then very slowly rotated to the required initial angle of tilt.

To commence the experiment the tank was quickly returned to a horizontal position so that the interface was then inclined at the original angle of tilt of the tank, simulating the tilted thermocline in a lake. The resulting flow was recorded on video and still photographs and the interface displacement measured by ultra-sonic wavegauges (Michallet & Barthélemy 1997). After the completion of the experiment, when the motion was considered to be once more quiescent, a final density profile was measured using a conductivity sensor and thermistor.

The experimental variables considered in this study, together with the resolution with which they were determined, were: the angle of tilt, θ ($\pm 0.03°$), the interface depth, h (± 0.2 cm), and the interface thickness, δ_ρ (± 0.2 cm). The overall density difference between the upper and lower layers was kept approximately constant at $\Delta\rho \approx 20\,\mathrm{kg\,m^{-3}}$ ($\pm 2\,\mathrm{kg\,m^{-3}}$). The angle of tilt was varied between $\theta = 0.125°$ and $\theta = 2.77°$, the upper limit being the maximum angle before the interface surfaced when the interface was at mid-depth. The depth ratios for the two-layer experiments ranged between $h/H = 0.2$ and $h/H = 0.5$. Each time the tank was filled with a particular interface depth a set of experiments was carried out with increasing angles of tilt. This resulted in a gradual thickening of the density interface over the set, typically from approximately 1 cm to 2 cm.

In the laboratory experiments the interface was generally below the mid-depth position so that the lower layer was the thinner layer. This is the reverse of the stratification found in most lakes in which the surface layer (epilimnion) is usually thinner than the lower layer (hypolimnion). However, this apparent reversal does not alter the physics of the system in the laboratory experiments (with a rigid lid and constant depth) and was necessary to accommodate the ultrasonic wavegauges. When referring to the laboratory experiments the layer suffix has been dropped, so that the thin layer is referred to simply as h.

3.2. *Experimental results*

When the initially tilted tank was returned to the horizontal the fluid immediately responded to the baroclinic pressure gradient, the lower layer flowing towards the downwelled end and the upper layer flowing in the opposite direction towards the upwelled end. Figure 4 shows a sequence of photographs from an experiment in which the initial basin-scale wave steepened into an internal surge which then evolved into a packet of solitons ($h/H = 0.3, \theta = 1.5°, \eta_0/h = 0.9$). The evolving wavefield is best observed by examining the time series of interfacial displacements recorded by the ultrasonic wavegauges, one of which was located near the centre of the tank ($x \approx 3.0$ m) and the others at the 1/4 and 3/4 positions ($x \approx 1.5, 4.5$ m). Any linear

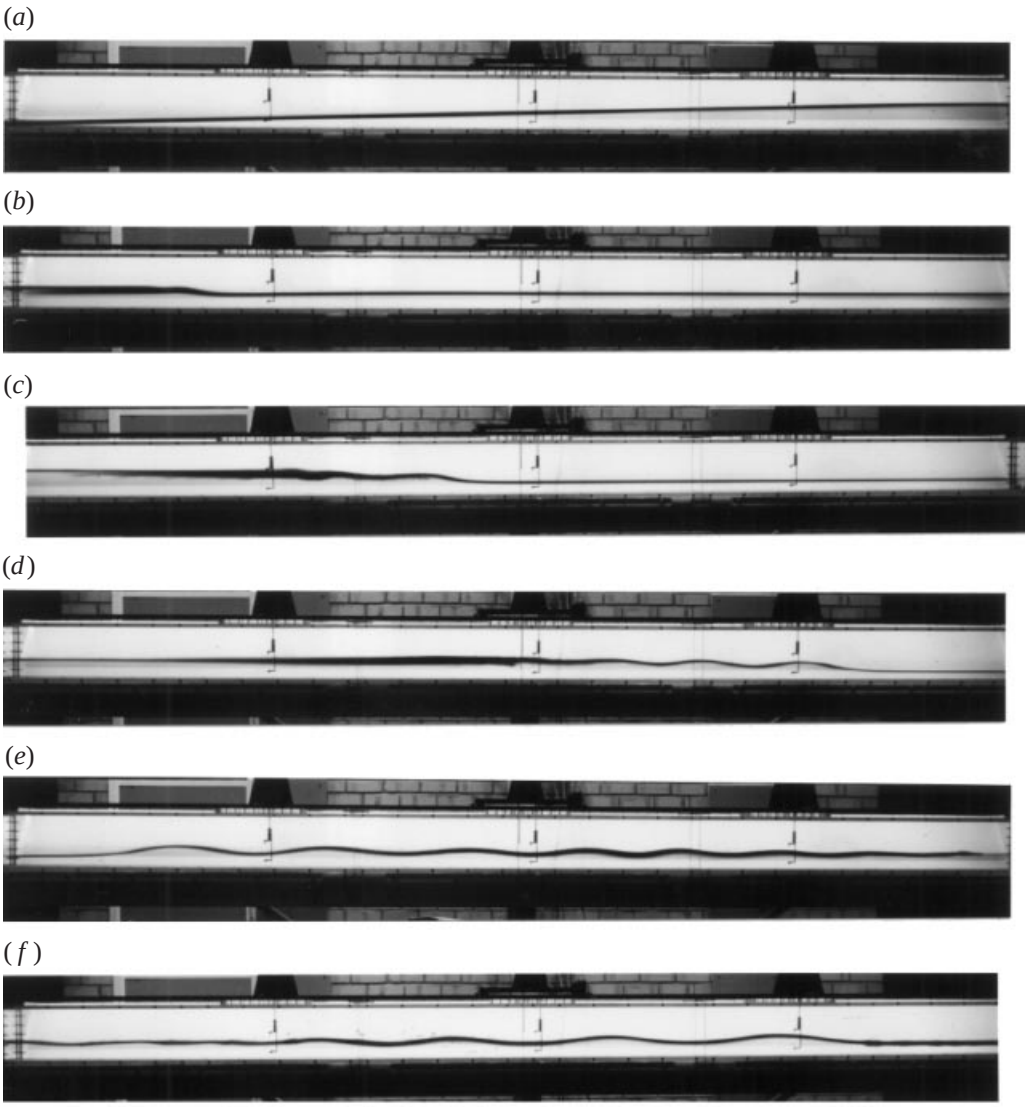

FIGURE 4. Photographs showing the steepening of an inital basin-scale wave to form a packet of solitons. The photographs show the whole 6 m length of the tank. The evolving train of solitons is propagating from left to right in panels (*b*)–(*d*), from right to left in panel (*e*) and from left to right in panel (*f*). ($h/H = 0.3, \theta = 1.5°, \eta_0/h = 0.9$).

basin-scale standing wave resulted in very small interfacial displacements near the central node, but caused much larger displacements at the 1/4 and 3/4 positions. The asymmetry introduced by any steepening of the basin-scale wave disrupted the standing wave pattern, increasing interfacial displacements at the centre of the tank. Figures 5 and 6 show typical time series from the wavegauge at the centre of the tank for a number of experiments with varying initial tilts and depth ratios.

In those experiments in which the nonlinearity was very weak (that is, for very small angles of tilt or when the interface was near the mid-depth) the interface oscillated as a basin-scale wave until the motion was damped by viscous effects. However, as the nonlinearity of the initial wave was increased (by increasing the angle of tilt or

by reducing the depth of the thinner layer), the initial basin-scale wave was observed to steepen and evolve into a train of solitons. In some experiments with large tilts or small depth ratios an undular bore was observed, sometimes with local shear instabilities and turbulence.

That the shorter waves are solitons that have evolved from the nonlinear steepening of the initial condition has been confirmed by the authors in a separate work (Horn *et al.* 2000).

Figure 2 plots the observations from the laboratory experiments on the regime diagram determined by the timescales developed in § 2. It can be seen that the experimental data generally comply with the regime classification. The points marked (A) showed signs of steepening but no solitons emerged before the wave was damped by boundary losses. The two points marked (B) lie just within Regime 4 when billows are expected but no billows were observed. This is most likely explained by the comment made in § 2.3 that (2.15) may underestimate the shear required to generate billows in an accelerating flow (Thorpe 1971). The point marked (C) was the only experiment in which bores and billows were observed and lies on the boundary of Regime 5. The experimental results confirm the general applicability of the timescale analysis and the regime classification, although the regimes in which supercritical flow is expected are poorly represented.

3.2.1. *Increasing the angle of tilt*

Figure 5 shows the effect of increasing the initial angle of tilt for a fixed interface depth ($h/H = 0.3$). For small angles of tilt ($\theta = 0.25^\circ$) the measured interfacial displacements were very small, due partly to the small amplitude of the wave but also because the wavegauge was located very near the central node of the basin-scale wave. In this case some steepening of the waveform was observed but no solitons emerged and the wave was damped by viscous effects. As the angle of tilt was increased to $\theta = 0.5^\circ$ the basin-scale wave was observed to steepen and evolve into a train of nonlinear waves. The evolution of these nonlinear waves can be followed in figure 5 as the waves repeatedly passed the wavegauge after reflecting from the ends of the tank. The emerging nonlinear waves were amplitude dispersive and we will refer to them as solitons. As predicted by the theory presented in § 2.4, as the angle of tilt was further increased the basin-scale wave was observed to steepen and evolve into solitons more quickly. The number and amplitude of the emerging waves increased with the amplitude of the initial basin-scale wave.

When the angle of tilt was sufficiently large ($\theta = 1.5^\circ$ for $h/H = 0.3$) the fluid in the thinner layer was seen to pile up at the downstream end of the tank and then propagate away from the wall as an internal bore. In figure 5(*e*) the central wavegauge signal shows the passage of an internal bore. The bore is undular but higher frequency components in the signal confirm that the bore was initially turbulent. The turbulence was observed to dissipate and the bore evolved into a train of large solitons. A comparison of the initial and final density profiles confirmed an increase in the potential energy of the system due to mixing by the bore. Similar internal bores were observed for the maximum tilt angles for each depth ratio. In all cases these bores quickly evolved into a packet of solitons. The waves propagated as waves of elevation from the downwelled end of the tank (recall that the lower layer is the thinner layer in the laboratory), except when the interface was at mid-depth when bores were observed propagating from both ends. Three of the observations of broken undular bores lie in Regime 2, indicating that these bores were generated by the rapid steepening of the basin-scale wave, not as a result of supercritical flow conditions.

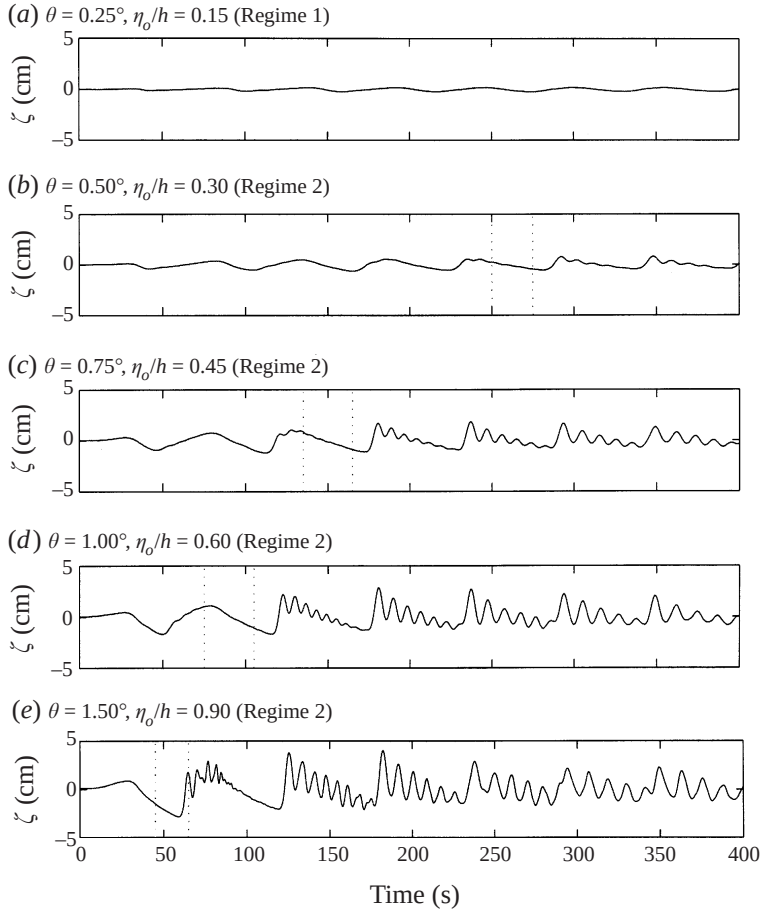

FIGURE 5. The nonlinearity of the system increases with increasing tilt angle. In these experiments the tilt angle θ determines the amplitude η_o of the initial basin-scale wave. As the angle of tilt increases, the initial wave is observed to steepen more quickly and the number and amplitude of the emerging solitary waves increases. The solitons were observed to emerge between the vertical dotted lines. The interfacial displacements measured by the wavegauge in the centre of the tank. For the time series shown $h/H = 0.3$ and $T_i = 109$ s.

3.2.2. *Decreasing the depth ratio*

Figure 6 shows the effect of increasing the nonlinearity of the system by reducing the thickness of the thinner layer h for a fixed initial angle of tilt $\theta = 0.5°$. When the interface was located at mid-depth it was observed to oscillate as a linear basin-scale wave and the measured interface displacements at the centre of the tank were very small. When the interface is at mid-depth, the nonlinear coefficients in (2.17) and (2.19) vanish, confirming that nonlinear steepening is not expected. However, when the interface was moved away from the mid-depth position the basin-scale wave was observed to steepen and evolve into nonlinear waves. As predicted by the theory presented in § 2.4, as the depth of the thinner layer was reduced the initial wave was observed to steepen more quickly and the number and amplitude of the emerging waves increased. In this way, increasing the nonlinearity of the system, either by increasing the amplitude of the initial disturbance or by reducing the depth of the thinner layer, was observed to have a similar effect.

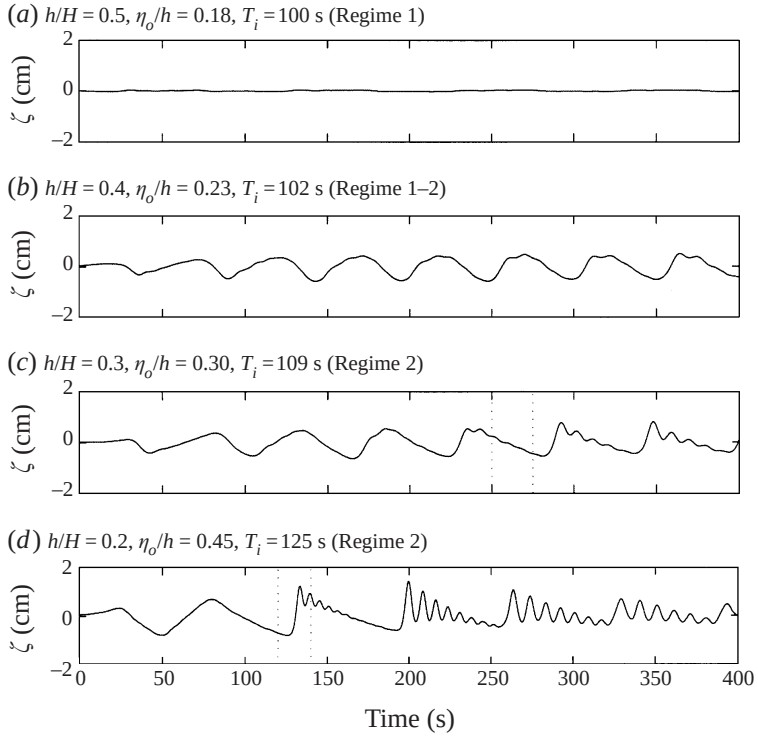

FIGURE 6. The nonlinearity of the system is increased as the depth ratio h/H decreases (as the thickness of the thinner layer is reduced). As the depth ratio is decreased, the initial wave is observed to steepen more quickly and the number and amplitude of the emerging solitons increases. The solitons were observed to emerge between the vertical dotted lines. For the time series shown $\theta = 0.5°$. The interfacial displacements were measured by the wavegauge in the centre of the tank.

3.2.3. *Steepening timescale*

The experimental time series were used to determine the constant of proportionality in (2.18). T_s is intended to be indicative of the time at which nonlinear steepening is balanced by dispersive effects. This should be accompanied by the first emergence of solitons from the steepening large-scale wave. We define the emergence of solitons as the time when the waves are sufficiently well separated that the depth (measured from the crest of the leading wave) of the trough between the leading solitons (measured from the crest of the leading wave) is 25% of the amplitude of the leading wave. Although this definition is somewhat arbitrary, it provides a consistent measure for comparing observations from different experiments and field studies. Figure 7 confirms that the constant of proportionality is 1. The error bars in figure 7 indicate that T_s is estimated to lie between observations at two wavegauges separated by 1.5 m or 3.0 m. The time during which solitons emerged is also shown on each of the time series in figures 5 and 6.

3.2.4. *Shear instabilities*

Shear instabilities induced by the basin-scale wave were only observed in one experiment in which the interface was at mid-depth and was inclined through the maximum angle ($h/H = 0.5$ and $\theta = 2.77°$). In other experiments in which the amplitude of the initial condition should have been sufficient for seiche-induced shear instabilities, it

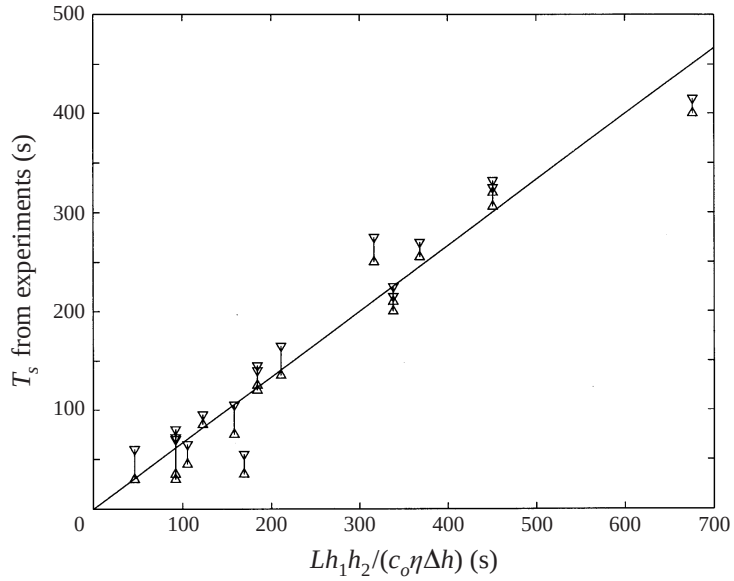

FIGURE 7. Observed times for the emergence of solitons and the steepening timescale T_s calculated using (2.18). Solitary waves usually emerged between wavegauges and the triangles indicate the observed times at which the leading soliton passed a wavegauge.

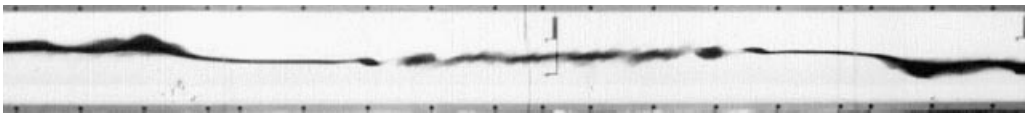

FIGURE 8. Photograph showing the collapse of Kelvin–Helmholtz billows in the centre of the tank while small bores propagate from each end. This was the only experiment in which billows were observed ($h_1/H = 0.5$, $\theta = 2.77°$).

appears that the formation of nonlinear waves extracted energy from the basin-scale wave, preventing billowing. In the experiment in which billows were observed, small bores also formed simultaneously at each end of the tank. However, since $h_1 \approx h_2$, the weakness of the nonlinearity in the system appears to have limited the transfer of energy from the basin-scale wave. Figure 8 shows the twin bores propagating towards the centre of the tank as the billows collapse. The formation of bores at both ends of the tank was only possible because of the symmetry of the stratification.

In some experiments large-amplitude surges and solitons were observed to generate localized shear instabilities as they propagated through the tank. These instabilities originated at the crest of the wave (always a wave of elevation in the laboratory set-up) and continued down the back face.

The mixing and enhanced dissipation caused by these wave-induced shear instabilities extracted energy from the soliton, reducing its amplitude to below the critical value (Bogucki & Garrett 1993).

Shear instabilities were also observed during the reflection of solitary waves from the vertical ends of the tank. When a train of solitons was reflected from the endwall it set up a pattern of standing waves that, when the interface was thin, induced shear instabilities at the nodes of the standing waves similar to those observed by Thorpe (1974).

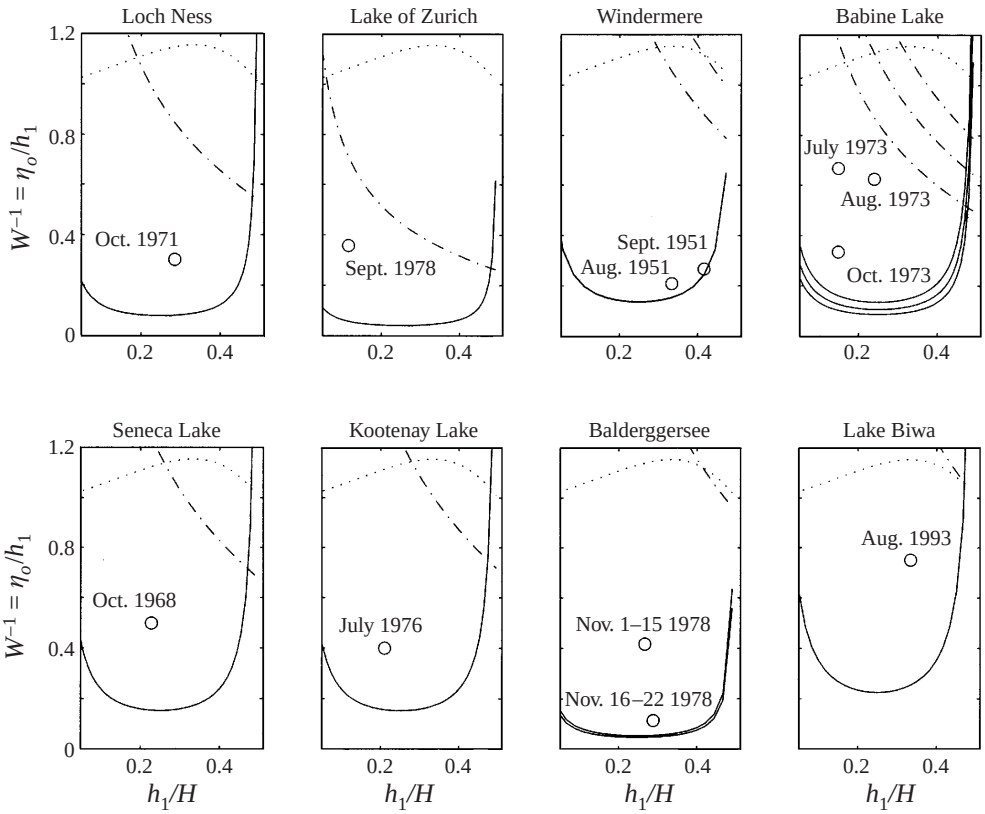

FIGURE 9. The field observations from table 1 are plotted on individual regime diagrams. The regime boundaries are determined separately for each lake by: $T_d = T_s$ (—), $T_b = T_i/4$ (···) and $T_{KH} = T_i/4$ (–·–·–). The value used for the sand grain roughness is $e = 6 \times 10^{-2}$ m.

4. Field observations

To determine the applicability of the analysis to real lakes we examined published observations from a number of lakes, most of which are narrow enough that the Earth's rotation is not expected to be significant, while in the last example in Lake Biwa the basin-scale response is a Kelvin wave. The various timescales described in § 2 have been calculated for each lake and the predicted degeneration mechanism is compared with field observations. The field observations are plotted on figure 9 and summarized in table 1.

Loch Ness is a long narrow deep lake that is aligned with the prevailing south-westerly wind. The internal seiche in Loch Ness has been observed to be highly nonlinear and often take the form of an internal surge or solitary waves (Thorpe, Hall & Crofts 1972; Thorpe 1977). We consider the data presented by Thorpe *et al.* (1972) relating to observations of what they describe as a typical surge observed on October 2–3 1971. A strong south-west wind ($> 13\,\mathrm{m\,s^{-1}}$) blew from the evening of September 30 until the afternoon of October 1 and then eased until it was calm on October 3. Thermistor records clearly show the arrival near the centre of the loch of an undular surge at 2200 h on October 2. The surge propagated towards the north-eastern end of the loch with a speed of $0.36\,\mathrm{m\,s^{-1}}$ and resembled a train of internal waves with a wavelength of about 1 km. Using the data from Thorpe

Lake	Dates	Observations	$W = \frac{h_1}{\eta_o}$	Regime
Loch Ness[a]	Oct. 2–3 1971	'*pronounced front or surge*'	3	2
Lake of Zurich[b]	Sept. 11–14 1978	'*steep fronted solitary wave*'	3	2
Windermere[c]	Aug. 14–20 1951	'*damped harmonic oscillations*'	5	1–2
	Sept. 13–17 1951	'*oscillatory waves*' with some steepening	3	1–2
Babine Lake[d]	July 5–10 1973	'*surges*'	2	2
	Aug. 12–15 1973	'*steep shock front*'	3	2
	Oct. 2–7 1973	'*surges*' and '*solitary waves*'	2	2
Seneca Lake[e]	Oct. 14–21 1968	'*surges*' consisting of trains of '*solitons*'	2	2
Kootenay Lake[f]	July 13–Aug. 17 1976	'*surges*' consisting of waves resembling '*solitons*'	2	2
Balderggersee[g]	Nov. 1–15 1978	'*asymetrical waves*'	9	2
	Nov. 16–22 1978	'*steepened wave front...described as an internal surge*'	2	2
Lake Biwa[h]	Sept. 4–13 1993	'*undular bores and solitary waves*'	1	2

TABLE 1. Examples of field observations, together with the calculated Wedderburn numbers and predicted regimes. Most of these lakes fall within Regime 2, in which nonlinear steepening is expected to dominate the degeneration of the initial seiche, except Windermere which lies near the boundary with Regime 1 in which the response is expected to be linear. (References: *a* Thorpe *et al.* (1972), *b* Mortimer & Horn (1982), *c* Heaps & Ramsbottom (1966), *d* Farmer (1978), *e* Hunkins & Fliegel (1973), *f* Wiegand & Carmack 1986, *g* Lemmin (1987), and *h* Saggio & Imberger (1998).)

et al. (1972) it can be seen that Loch Ness falls clearly within Regime 2 over this period ($T_{KH} > T_i/4$, $T_b > T_i/4$, $T_s < T_d$) and so we would expect to see the initial basin-scale seiche steepen and evolve into a train of solitons. Our timescale analysis supports previous interpretations that the undular surge observed in Loch Ness is generated by the nonlinear steepening of a basin-scale wave.

Mortimer & Horn (1982) present data from thermistor chains at five stations along the length of the Lake of Zurich. They suggest that the thermistor records from September 1978 show an internal surge generated by the interaction of the downwelling thermocline with the end of the lake. A strong wind blew towards the southern end of the lake until midday on September 12, tilting the thermocline over the length of the lake. After the wind dropped a strong surge was recorded propagating southwards from the northern end of the lake and solitary waves were seen to evolve (Mortimer & Horn (1982) also comment on a smaller surge propagating north before the wind ceased, which was probably generated during the set-up of the thermocline).

To investigate the possible generation mechanisms for the observed internal surge we consider the degeneration timescales calculated from the data in Mortimer & Horn (1982). Calculations show that $T_b > T_i/4$ so that the observed surge is unlikely to have been an internal bore generated by the mechanism described in § 2.5. However, $T_s < T_d$ so that the initial basin-scale wave would steepen and evolve into solitary waves, and since $T_i > T_s > T_i/2$, the solitary waves would be expected to emerge propagating southwards, as observed.

Heaps & Ramsbottom (1966) applied their analytical linear two-layer model to Windermere and showed that the results compared well with field data. Together with the observation that the dominant response of the lake is a damped basin-scale wave,

this suggests that nonlinear effects do not play an important role in Windermere. Table 1 presents observations and the regime for Windermere using the data presented by Heaps & Ramsbottom (1966) for two periods: August 14–20 and September 13–17, 1951. We see that $T_{KH} > T_i/4$ and $T_b > T_i/4$, so that neither seiche-induced shear instabilities nor internal bores are expected to occur. However, $T_i < T_s < T_d$ suggesting that we would see the initial basin-scale seiche gradually steepen over about two periods, although the waves would also be substantially damped during this time. The plots presented in Heaps & Ramsbottom (1966) show some steepening of the basin-scale wave but there is no evidence of solitary waves emerging.

Farmer (1978) describes observations of long nonlinear internal waves and surges in Babine Lake. These surges took the form of a train of short-period waves which were identified as solitons. The timescale comparison shows that Babine Lake lies in Regime 2, supporting the conclusion by Farmer (1978) that the solitons are generated by the nonlinear steepening of an initial depression of the thermocline at the southern end of the lake. In the case of Babine Lake, the variable width of the lake is also expected to effect the rate of steepening; the narrower section approximately halfway along the lake would enhance steepening.

Although the timescale derivations do not include rotational effects, the internal wave spectra and thermistor records from Lake Biwa motivated aspects of this study so we include it here. For the purposes of this analysis we assume that the basin-scale Kelvin wave steepens as it travels along the perimeter of the lake in an equivalent way to the steepening of a non-rotating seiche. The results of spectral analysis and numerical modelling presented by Saggio & Imberger (1998) confirmed that the basin-scale response of the lake was composed of Kelvin and Poincaré waves and that these waves are energized directly by the wind. However, following the passage of a storm, a high-frequency peak also appeared in the spectra which was attributed to undular bores and solitons evident in the thermistor record. The timescale comparison shows that Lake Biwa falls within Regime 2, suggesting that these high-frequency nonlinear waves might be associated with the steepening of the basin-scale Kelvin wave. The evolution of nonlinear waves in rotating systems is sufficiently different (e.g. Fedorov & Melville 1995), however, to require further investigation before this analysis can be extended to include rotating systems.

Table 1 also includes the degeneration timescales for Seneca Lake, Kootenay Lake and Balderggersee. These lakes all display a highly nonlinear response to moderately strong wind events and internal surges are predicted by the comparison of timescales.

5. Discussion

The laboratory experiments presented in § 3 together with the field observations described in § 4 confirm the applicability of the proposed timescale analysis and regime classification. The analysis suggests that most lakes fall within Regime 2, in which nonlinear steepening is expected to dominate the degeneration of an initial basin-scale wave. Furthermore, nonlinear effects are likely to be important in characterizing a lake's initial response to an applied wind stress.

Regime 1, in which the initial basin-scale wave is damped as quickly as it can steepen, applies only to very small-amplitude seiches. For the lakes considered in § 4, except Windermere, wind events of duration $T_i/4$ with wind speeds exceeding 3–4 m s^{-1} would generate basin-scale waves that would steepen into solitons. However, in the case of Windermere, the greater depth of the thermocline relative to the overall

depth ($h_1/H = 0.4$) means that the response will remain linear for wind speeds up to 7–10 m s^{-1}.

Although it is possible to generate seiche-induced shear instabilities in the laboratory (in extreme cases), field observations of such events are rare; observed shear instabilities are usually associated with large-amplitude surges and solitons. Shear instabilities (Regime 4) were found to be restricted to large-amplitude seiches when the interface is near mid-depth. Other waves, either generated during the initial set-up of the thermocline or after the removal of the wind stress, steepen and evolve into solitons before billows develop.

Previous field studies have described the evolution and propagation of internal surges in many lakes. In the laboratory and field data examined, our analysis suggests that the observed internal surges were all generated by the nonlinear steepening of an initial wave (Regime 2). The initial seiche amplitude required to generate the supercritical flow necessary for the formation of an internal bore (Regime 3) corresponds to upwelling of the thermocline which was not observed in the cases considered. As described in § 2.7, such upwelling events lead to the development of a highly nonlinear density front, accompanied by turbulent mixing, horizontal dispersion and deepening of the surface layer, all of which extract energy from the initial condition and generally disrupt wave evolution and propagation. We conclude that the internal surges so often observed are generated by nonlinear steepening.

5.1. *Energetics of nonlinear steepening*

The generation of solitons by nonlinear steepening in Regime 2 results in a transfer of energy from the basin scale to much smaller scales. Internal wave spectra from Lake Biwa Imberger (1994) clearly show that major wind events result in an increase in the energy of basin-scale waves and an increase in the energy at smaller scales, near the buoyancy frequency. Saggio & Imberger (1998) postulated that these high-frequency waves were the result of interaction of the basin-scale waves with the lake bathymetry. The analysis presented above suggests that these high-frequency waves also include internal surges and solitons generated by the nonlinear steepening of the initial basin-scale wave. Hutter *et al.* (1998) also found that nonlinear effects were responsible for many of the small-scale features observed in the internal wavefield of other lakes.

The temporal development of the internal wave spectra of the laboratory experiments was examined using a continuous wavelet transform. Figure 10 shows the time–frequency plot for one experiment in which the basin-scale wave was seen to steepen and evolve into a train of solitons. The energy transfer from low to higher frequencies coincides with the emergence of the solitons. Importantly though, energy appears to be transferred directly from the basin-scale wave to the solitons at about $t = 200$ s ($T_s = 210$ s for this experiment). Although there is some energy at wavelengths separating the initial basin-scale wave and the emerging solitary waves, there is no evidence of energy cascading through these intermediate scales. In the internal wave spectra for lakes, the low-frequency basin-scale waves and the high-frequency solitons are more widely separated. However, nonlinear steepening is not expected to contribute to the generation of waves in the intermediate ω^{-2} range or to the maintenance of the apparently universal spectral shape; the source of these waves is an important outstanding issue.

The transfer of energy within the internal wave spectrum from the basin scale to smaller scales has important consequences for the subsequent cascade of energy to turbulent scales. Internal solitons can induce large shears that can lead to localized

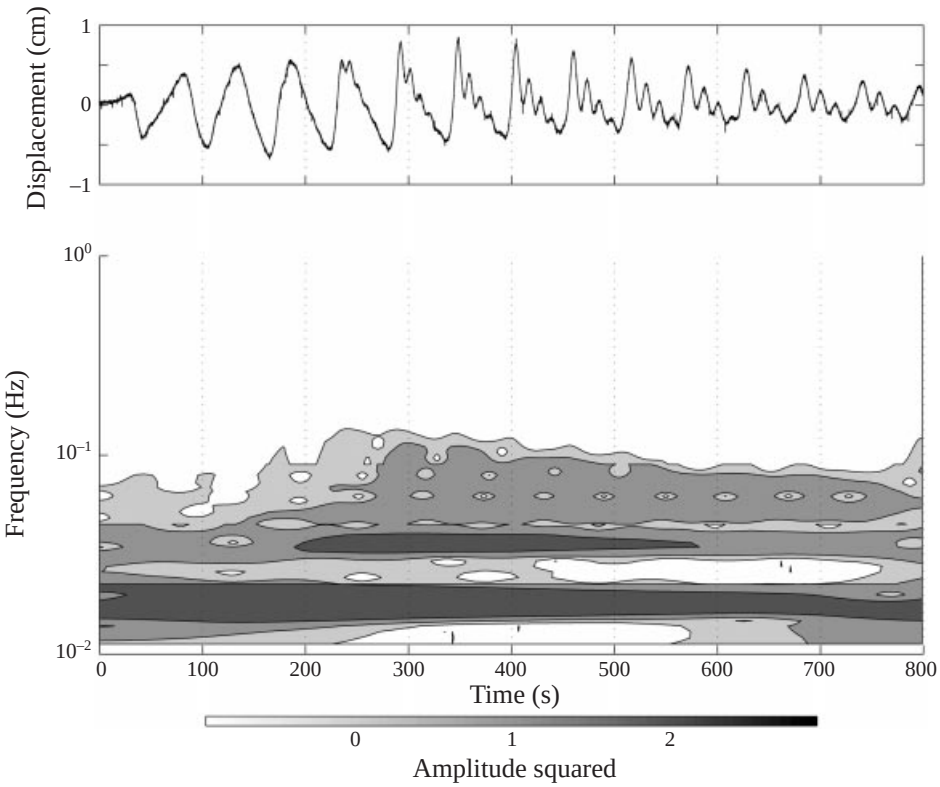

FIGURE 10. Time–frequency analysis of a laboratory nonlinear steepening event. The upper panel shows the interface displacement measured by a wavegauge in the centre of the tank. The lower panel shows the time-varying energy spectra calculated using a continuous wavelet transform. For this experiment $h_2/H = 0.3$ and $\theta = 0.5^\circ$ (see figure 5*b*).

shear instabilities and breaking. Although the total energy of a wave is approximately constant during steepening, the reduction in horizontal lengthscale acts to increase the energy density of the wave, increasing the likelihood of breaking. This was observed in our laboratory experiments and has been recorded in Loch Ness (Thorpe 1977) and the Lake of Zurich (Mortimer & Horn 1982). These local shear instabilities result in turbulent patches in the interior of the lake with locally increased dissipation and mixing. However, energy is only extracted from the solitary waves until they decay below a critical amplitude (Bogucki & Garrett 1993).

A more significant feature in terms of energy dissipation is the shoaling of solitons at sloping boundaries (Helfrich 1992; Michallet & Ivey 1999). Michallet & Ivey (1999) have shown that solitary waves lose up to 70% of their energy in a single reflection from typical lake slopes. This explains the observation of Saggio & Imberger (1998) that the high-frequency peaks in the internal wave spectra are very short-lived. Whereas an initial basin-scale wave would be reflected from the sloping ends of a lake (since to these waves the boundaries appear very steep), the transfer of energy from the basin-scale wave to shorter solitons causes most of the energy to be quickly dissipated at the boundaries, increasing the overall rate of dissipation. In this way, breaking solitons are a source of energy for mixing in the benthic boundary layer, which has important implications for water quality in lakes. The timescale for the formation of solitons determines where and in what direction the solitons emerge

and, hence, where the waves will shoal and dissipate their energy. This suggests that the benthic boundary layer will not be uniform around the perimeter of a lake, but will be more active in regions where solitons first shoal.

The generally accepted picture of the processes leading to the tilting of the thermocline during a wind event is based on linear analysis (e.g. Heaps & Ramsbottom 1966; Spigel & Imberger 1980). However, numerical modelling has demonstrated the importance of nonlinear effects in the initial response of a lake to an applied wind stress (Hutter *et al.* 1998), a conclusion confirmed by the results presented here. The effects of seiching on processes such as mixed-layer deepening (Spigel 1980) should be re-examined to include the degeneration of these basin-scale waves due to nonlinear steepening.

The laboratory experiments and analysis for this study did not include the effects of topography. As well as the role played by sloping boundaries in the dissipation of internal wave energy, the sloping ends of a lake and features such as sills and contractions are all likely to enhance the steepening of basin-scale waves, reducing the time taken for the emergence of solitons. The generation of the internal surge by the interaction of the downwelling thermocline with the sloping boundary postulated by Mortimer & Horn (1982) may well be an example of topographic enhancement of nonlinear steepening.

5.2. *Implications for modelling and data analysis*

The significant role played by nonlinear steepening and solitons in the degeneration of basin-scale internal waves also has implications for the way in which we model the hydrodynamics of such systems. Most numerical models employed to study the hydrodynamics of lakes make the hydrostatic approximation. While these models have been used to satisfactorily simulate most flows, by neglecting vertical accelerations they are unable to capture the evolution and propagation of solitons and therefore the transfer of energy from the basin-scale seiche to these shorter waves. These models will be unable to predict the subsequent rapid dissipation and mixing caused by shoaling solitary waves, the location and timing of which may be important in determining water quality. It is important to quantify the energetics of nonlinear steepening in lakes to determine the significance of this omission from this large class of numerical models.

6. Conclusions

We set out to investigate one aspect of the energy cascade in lakes – the degeneration of basin-scale interfacial waves. By identifying a number of possible mechanisms and comparing the timescales over which they act, regimes have been identified in which particular mechanisms are expected to dominate the degeneration of an initial basin-scale internal wave. Predictions based on this comparison of timescales have been shown to compare well with both laboratory experiments and field observations. Most lakes are expected to fall within Regime 2, in which nonlinear steepening of the initial basin-scale wave results in the generation of solitons.

We can now add to the description of the evolution of the internal wave spectrum proposed by Saggio & Imberger (1998) by including the effects of nonlinear steepening. The main source of energy for the internal wavefield is the action of the wind blowing over the surface of the lake, generating low-frequency basin-scale waves. These basin-scale waves may interact with the lake bathymetry to generate higher-frequency waves. However, in most lakes the basin-scale waves also steepen

due to nonlinear effects, evolving into internal surges and solitons with much shorter lengthscales and higher frequencies. These solitons are short-lived, shoaling and breaking at the sloping boundaries, transferring most of their energy to turbulence in the benthic boundary layer. In this way, nonlinear steepening enhances the transfer of energy from the initial basin-scale waves to the turbulent benthic boundary layer. The fraction of energy cascaded through solitons by this mechanism has yet to be quantified but is important in determining the overall energy flux path in lakes. The energy transfers accompanying nonlinear steepening are directly from the basin scale to the solitons and not through intermediate wavelengths. The mechanisms that maintain the observed ω^{-2} slope of the internal wave spectra in most lakes remain to be identified.

Following a wind event, the steepening timescale T_s determines where and in which direction solitons first emerge from the initial seiche. In some lakes solitons are observed to propagate in only one direction and hence shoal at only one end of the lake. This suggests that the turbulent benthic boundary layer would be more active at the end where shoaling occurs, with important implications for the spatial variability of water quality in those lakes.

The derivation of the various degeneration timescales considered did not include the effects of rotation or of higher vertical modes. However, it would be possible to derive appropriate timescales for both of these effects in order to extend the description to include lakes in which rotation can no longer be ignored or in which the two-layer approximation is no longer valid. Furthermore, the analysis excluded topographic effects which are expected to play an important role in determining the rate of steepening of an initial basin-scale internal wave.

The evolution, propagation and shoaling of solitons appear to be important processes in most lakes and yet they are not captured by numerical models that use the hydrostatic approximation. Further work should be undertaken to quantify the energy transfers associated with these processes so that the significance their omission can be determined.

The authors are grateful to Larry Redekopp, Kraig Winters and Herve Michallet for their discussions on this work, and to Angelo Saggio for the wavelet analysis and Lake Biwa data. This research was supported by the Centre for Environmental Fluid Dynamics and the Australian Research Council and was completed while the first author was a recipient of an Australian Postgraduate Award and a Samaha Research Scholarship. This paper is Centre for Water Research reference ED 1371 DH.

REFERENCES

Batchelor, G. K. 1967 *An Introduction to Fluid Dynamics*. Cambridge University Press.

Bogucki, D. & Garrett, C. 1993 A simple model for the shear-induced decay of an internal solitary wave. *J. Phys. Oceanogr.* **28**, 1767–1776.

Corcos, C. M. & Sherman, F. S. 1976 Vorticity concentration and the dynamics of unstable free shear layers. *J. Fluid Mech.* **73**, 241–264.

Farmer, D. M. 1978 Observations of long nonlinear internal waves in a lake. *J. Phys. Oceanogr.* **8**, 63–73.

Fedorov, A. V. & Melville, W. K. 1995 Propagation and breaking of nonlinear Kelvin waves. *J. Phys. Oceanogr.* **25**, 2518–2531.

Hammack, J. L. & Segur, H. 1974 The Korteweg–de Vries equation and water waves. Part 2. comparison with experiments. *J. Fluid Mech.* **65**, 289–314.

Hammack, J. L. & Segur, H. 1978 Modelling criteria for long water waves. *J. Fluid Mech.* **84**, 359–373.

Heaps, N. S. & Ramsbottom, A. E. 1966 Wind effects on the water in a narrow two-layered lake. *Phil. Trans. R. Soc. Lond.* A **259**, 391–430.

Helfrich, K. R. 1992 Internal solitary wave breaking and run-up on a uniform slope. *J. Fluid Mech.* **243**, 133–154.

Horn, D. A., Imberger, J., Ivey, G. N. & Redekopp, L. G. 2000 A weakly nonlinear model of long internal waves in lakes. In *Proc. 5th Intl Symp. on Stratified Flows* (ed. G. A. Lawrence, R. Pieters & N. Yonemitsu), vol. 1, pp. 331–336. University of British Columbia.

Hunkins, K. & Fliegel, M. 1973 Internal undular surges in Seneca Lake: A natural occurrence of solitons. *J. Geophys. Res.* **78**, 539–548.

Hutter, K. 1991 Large scale water movements in lakes. *Aquatic Sci.* **53**, 100–135.

Hutter, K., Bauer, G., Wang, Y. & Güting, P. 1998 Forced motion response in enclosed lakes. In *Physical Processes in Lakes and Oceans* (ed. J. Imberger). AGU.

Imberger, J. 1985 The diurnal mixed layer. *Limnol. Oceanogr.* **30**, 737–770.

Imberger, J. 1994 Transport processes in lakes: A review. In *Limnology Now: A Paradigm of Planetary Problems* (ed. R. Margalef). Elsevier.

Ivey, G. N. & Nokes, R. I. 1989 Vertical mixing due to the breaking of critical internal waves on sloping boundaries. *J. Fluid Mech.* **204**, 479–500.

Keulegan, G. H. 1959 Energy dissipation in standing waves in rectangular basins. *J. Fluid Mech.* **6**, 33–50.

Lemmin, U. 1987 The structure and dynamics of internal waves in Baldeggersee. *Limnol. Oceanogr.* **32**, 43–61.

Lighthill, M. J. 1978 *Waves in Fluids*. Cambridge University Press.

Long, R. R. 1972 The steepening of long internal waves. *Tellus* **24**, 88–99.

Michallet, H. & Barthélemy, E. 1997 Ultrasonic probes and data processing to study interfacial solitary waves. *Exps. Fluids* **22**, 380–386.

Michallet, H. & Ivey, G. N. 1999 Experiments on mixing due to internal solitary waves breaking on uniform slopes. *J. Geophys. Res.* **104**, 13,467–13,478.

Monismith, S. G. 1986 An experimental study of the upwelling response of stratified reservoirs to surface shear stress. *J. Fluid Mech.* **171**, 407–439.

Monismith, S. G. 1987 Modal response of reservoirs to wind stress. *J. Hydraul. Engng* **113**, 1290–1306.

Mortimer, C. H. 1952 Water movements in lakes during summer stratification; evidence from the distribution of temperature in Windermere. *Phil. Trans. R. Soc. Lond.* B **236**, 355–404.

Mortimer, C. H. 1974 Lake hydrodynamics. *Mitt. Intl Verein. Limnol.* **20**, 124–197.

Mortimer, C. H. & Horn, W. 1982 Internal wave dynamics and their implications for plankton biology in the Lake of Zurich. *Vierteljahresschr. Naturforsch. Ges. Zurich* **127**(4), 299–318.

Saggio, A. & Imberger, J. 1998 Internal wave weather in a stratified lake. *Limnol. Oceanogr.* **43**, 1780–1795.

Spigel, R. H. 1978 Wind mixing in lakes. PhD thesis, University of California, Berkeley.

Spigel, R. H. 1980 Coupling of internal wave motion with entrainment at the density interface of a two-layer lake. *J. Phys. Oceanogr.* **10**, 144–155.

Spigel, R. H. & Imberger, J. 1980 The classification of mixed-layer dynamics in lakes of small to medium size. *J. Phys. Oceanogr.* **10**, 1104–1121.

Stevens, C. & Imberger, J. 1996 The initial response of a stratified lake to a surface shear stress. *J. Fluid Mech.* **312**, 39–66.

Stevens, C., Lawrence, G., Hamblin, P. & Carmack, E. 1996 Wind forcing of internal waves in a long narrow stratified lake. *Dyn. Atmos. Oceans* **24**, 41–50.

Stocker, T. & Hutter, K. 1987 *Topographic Waves in Channels and Lakes on the f-plane*. Springer.

Thompson, R. O. R. Y. & Imberger, J. 1980 Response of a numerical model of a stratified lake to wind stress. In *Second Intl Symp. on Stratified Flows*, *Trondheim* (ed. T. Carstens & T. McClimans). Tadir, Trondheim.

Thorpe, S. A. 1968 On standing internal gravity waves of finite amplitude. *J. Fluid Mech.* **32**, 489–528.

Thorpe, S. A. 1971 Experiments on the instability of stratified shear flows: miscible fluids. *J. Fluid Mech.* **46**, 299–319.

THORPE, S. A. 1974 Near-resonant forcing in a shallow two-layer fluid: a model for the internal surge in Loch Ness. *J. Fluid Mech.* **63**, 509–527.

THORPE, S. A. 1977 Turbulence and mixing in a Scottish loch. *Phil. Trans. R. Soc. Lond.* A **286**, 125–181.

THORPE, S. A. 1998 Some dynamical effects of the sloping sides of lakes. In *Physical Processes in Lakes and Oceans* (ed. J. Imberger). AGU.

THORPE, S. A., HALL, A. & CROFTS, I. 1972 The internal surge in Loch Ness. *Nature* **237**, 96–98.

THORPE, S. A., HALL, A. J., TAYLOR, C. & ALLEN, J. 1977 Billows in Loch Ness. *Deep-Sea Res.* **24**, 371–379.

THORPE, S. A., KEEN, J. M., JIANG, R. & LEMMIN, U. 1996 High-frequency internal waves in Lake Geneva. *Phil. Trans. R. Soc. Lond.* A **354**, 237–257.

WIEGAND, R. C. & CARMACK, E. 1986 The climatology of internal waves in a deep temperate lake. *J. Geophys. Res.* **91**, 3951–3958.

WOOD, I. R. & SIMPSON, J. E. 1984 Jumps in layered miscible flows. *J. Fluid Mech.* **140**, 329–342.

WOODS, J. D. 1968 Wave-induced shear instability in the summer thermocline. *J. Fluid Mech.* **32**, 791–800.

WU, J. 1977 A note on the slope of a density interface between two stably stratified fluids under wind. *J. Fluid Mech.* **81**, 335–339.